PHYSICAL REVIEW B **94**, 205308 (2016)

Slow light and slow acoustic phonons in optophononic resonators

V. Villafañe,[1] P. Soubelet,[1] A. E. Bruchhausen,[1] N. D. Lanzillotti-Kimura,[2] B. Jusserand,[3] A. Lemaître,[2] and A. Fainstein[1,*]

[1]*Centro Atómico Bariloche and Instituto Balseiro, CONICET, CNEA, 8400 S.C. de Bariloche, Bariloche, Argentina*

[2]*Centre de Nanosciences et de Nanotechnologies, Centre National de la Recherche Scientifique, Université Paris-Sud, Université Paris-Saclay, C2N Marcoussis, 91460 Marcoussis, France*

[3]*Institut des NanoSciences de Paris, UMR 7588, Centre National de la Recherche Scientifique, Université Pierre et Marie Curie, 75015 Paris, France*

(Received 25 July 2016; revised manuscript received 4 November 2016; published 28 November 2016)

Slow and confined light have been exploited in optoelectronics to enhance light-matter interactions. Here we describe the GaAs/AlAs semiconductor microcavity as a device that, depending on the excitation conditions, either confines or slows down both light and optically generated acoustic phonons. The localization of photons and phonons in the same place of space amplifies optomechanical processes. Picosecond laser pulses are used to study through time-resolved reflectivity experiments the coupling between photons and both confined and slow acoustic phonons when the laser is tuned either with the cavity (confined) optical mode or with the stop-band edge (slow) optical modes. A model that fully takes into account the modified propagation of the acoustic phonons and light in these resonant structures is used to describe the laser detuning dependence of the coherently generated phonon spectra and amplitude under these different modes of laser excitation. We observe that confined light couples only to confined mechanical vibrations, while slow light can generate both confined and slow coherent vibrations. A strong enhancement of the optomechanical coupling using confined photons and vibrations, and also with properly designed slow photon and phonon modes, is demonstrated. The prospects for the use of these optoelectronic devices in confined and slow optomechanics are addressed.

DOI: 10.1103/PhysRevB.94.205308

I. MOTIVATION

Optomechanical resonators [1–11] are at the base of many new fundamental ideas related to the generation and study of quantum macroscopic states [12–15], and for the most advanced strategies for displacement measurements below the standard quantum limit [16], with applications, for example, in gravitational waves detection [17]. Optomechanical cooling down to the quantum ground state of mechanical motion and stimulated emission of vibrations [18,19] are some of the demonstrated consequences of so-called dynamical back-action in these devices. Large spatial overlap and an efficient coupling mechanism between photons and phonons are required to optimize these processes. In addition, long lifetimes in the same shared space are required to increase the optomechanical cooperativity in the coupled dynamics. This is typically accomplished through the use of cavities that resonantly confine photons and phonons. In this paper we address the possibility of slowing down light and acoustic phonons as an alternative to confinement. As a model system to study this perspective, we describe the properties of GaAs/AlAs microcavities as devices that can either confine or slow down photons and phonons in the same place of space, coupling photons with phonons efficiently, and allowing for the excitation of high-frequency nano-optomechanical modes in the technologically relevant 20–100-GHz range.

Semiconductor optical microcavities based on distributed Bragg reflectors (DBRs) have been and continue to be the subject of intense research due to the fascinating and rich physics of cavity polaritons [20–22], as single and entangled photon emitters for quantum optics when combined with quantum dots [23,24], and as the basis for efficient lasers [25]. In the domain of nanophononics these devices have also caught the attention from the early times of the field for strongly enhanced (10^5–10^7) Raman scattering spectroscopy of phonons [26–29]. More recently they have been proposed as a means to amplify either the phonon generation, the detection, or both, in picosecond acoustics experiments [30,31]. Microcavities can be strongly modulated by the strain associated to phonons generated by ultrashort laser pulses. Such phonons can be injected into the cavity from the outside [32–36], or generated within the resonator by laser pulses coupled to the optical cavity mode [37,38]. It has been recently demonstrated [37] that optical GaAs/AlAs based microcavities constitute optimized resonators that confine in the same place of space near infrared light and GHz-THz acoustic phonons. These latter confined acoustic phonons correspond to nano-optomechanical modes that strongly modulate the optical cavity mode, thus strongly enhancing the photon-phonon coupling processes [37–40].

The DBRs used as mirrors for the described microresonators are an example of one-dimensional photonic crystals, structures that are interesting by themselves. In fact, the wavelength scale periodicity leads to the formation of photon bands with the concomitant opening of band gaps and strong modification (particularly slowing down) of the light group velocity at the stop-band edges [41–43]. Slow light in such devices has been used to enhance light-matter interactions. It has been used to modify light absorption and emission [44,45], to enhance nonlinearities as sum-frequency generation and phase modulation both in solids and molecules [46–50] for efficient lasing [51,52], and to amplify the interaction of light with vibrations in Raman processes [53–55]. In the domain of acoustics, coherent phonon generation has been studied in

*Email:afains@cab.cnea.gov.ar

opals, evidencing a dependence of the generation efficiency on the tuning between the light wavelength and the optical band gap of these periodic structures [56]. Very recently, the simultaneous guiding of slow elastic and light waves in three-dimensional phoxonic crystals with a line defect has been theoretically proposed [57]. The question then arises: how do slow photons and slow acoustic phonons perform with a perspective in optomechanics in these modulated dielectric structures? This question becomes particularly relevant in view of recent reports of photon lifetimes extended to the millisecond range (lifetimes that are characteristic of phonons) by introducing slow light effects in a whispering gallery mode microresonator [58].

With this application in mind, we study here in detail DBR-based GaAs/AlAs microcavities as structures that present both light confinement and slowing down, depending on whether the laser is tuned to the cavity or stop-band edge modes. Interestingly, precisely the same happens for acoustic phonons, and thus these devices are a rich playground to investigate confined and slow optomechanical effects. We study these structures through time-resolved coherent phonon generation experiments using picosecond lasers. The coupling of both confined and slow light to the different confined and extended acoustic phonons is studied, and the role of the different coupling mechanisms involved is addressed.

II. SAMPLE AND EXPERIMENTAL SETUP

We consider a $\lambda/2$ GaAs-spacer planar vertical microcavity with $Al_{0.18}Ga_{0.82}As$ /AlAs $\lambda/4,\lambda/4$ DBRs, 20 pairs of layers on the bottom, 18 on top, grown on a GaAs substrate as described in Refs. [59,60]. A scheme of the structure is presented in the bottom panel of Fig. 1. The sample had a small wedge to allow for the tuning of the cavity mode energy by displacing the laser spot on the sample surface. As we have demonstrated previously, this structure performs as an optomechanical resonator that simultaneously confines photons and acoustic phonons of the same wavelength [37,38]. The point made here is that, besides this simultaneous electromagnetic and elastic confinement, the structure also slows down both light and phonons. To illustrate this we show in Fig. 1(a) a calculated *optical* reflectivity, where the cavity and edge modes are indicated. The spatial distribution of the electric-field intensity associated to these two kind of modes is shown in panel (c). It was obtained considering a plane-wave incident from the air, with a unitary amplitude. The confined and DBR character of the modes is apparent. The value of the field in air is the same for both modes; this is not visible in the figure because we had to divide the cavity mode by a factor 50 because it is strongly amplified by cavity effect. The edge modes (name used in the sense that they appear at the edge of the reflectivity stop bands) correspond to standing waves arising from the Bragg reflection at the Brillouin-zone center and edge. As a consequence of this the photon dispersion flattens, reflecting a reduction of the wave group velocity [41]. The localization (standing-wave character) of the edge modes within the DBRs is a signature of this light speed reduction. Naturally these same effects of light and sound slowing down exist in a simple DBR. Here, we study a microcavity (two

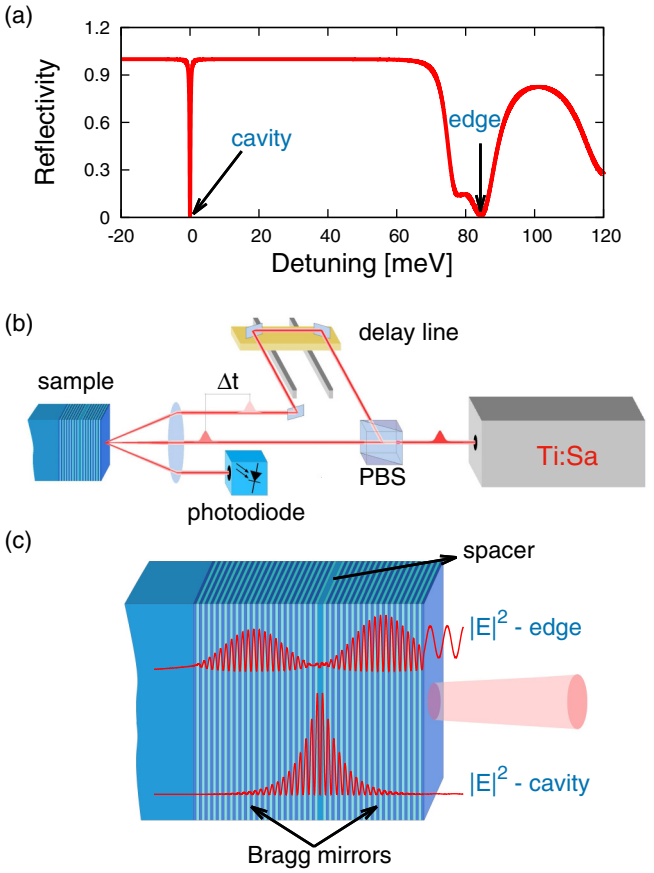

FIG. 1. (a) Calculated optical reflectivity of the microcavity device. Energies are given with respect to the cavity mode. Cavity and edge modes are indicated. (b) Time-resolved reflectance difference experimental setup. PBS stands for polarizing beam splitter. (c) Calculated spatial distribution of the electric field associated to the cavity (confined) and edge (slow) modes for incidence from the air side (the edge mode has been multiplied by a factor 50 for clarity). Note that figures essentially identical to (a) and (c) are obtained when evaluating the phononic reflectivity and spatial distribution of the strain fields of the longitudinal acoustic phonon displacement associated to the cavity and edge phonon modes.

DBRs enclosing a spacer layer), a structure readily available in many laboratories, because it allows for the simultaneous experimental test of photon-phonon confinement and speed reduction. A discussion involving bare DBRs will be provided at the end of this paper.

Free-surface boundary conditions in mechanics lead to total reflectivity at the structure-air surface. Consequently, an *acoustic* reflectivity similar to that shown for light in Fig. 1(a) cannot be defined. An equivalent way to present the phononic problem can be obtained evaluating the surface displacement as a function of phonon frequency for a mechanical wave incident from the substrate side [61]. Such a curve reflects essentially the device phonon transmission, which for the structure considered here (no absorption) turns out to be almost identical to the inverse of the reflectivity shown in Fig. 1(a). Acoustic stop bands appear, with perfectly centered confined phonon modes, and limited by edge states, with essentially the same mode distribution as for light in Fig. 1(c) [62].

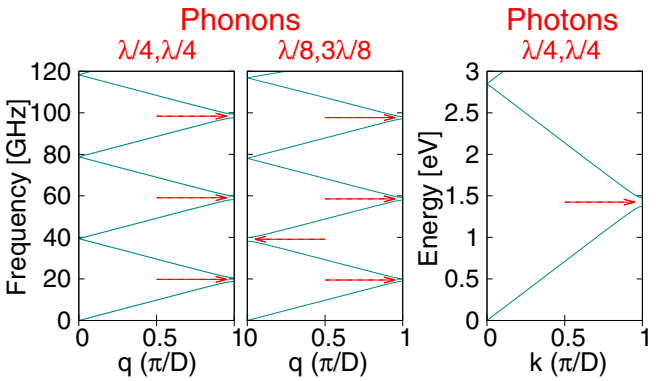

FIG. 2. Photon and phonon dispersion of a periodic $Al_{0.18}Ga_{0.82}As$ /AlAs multilayer. The left and right panels correspond to the phononic and photonic dispersion of $\lambda/4,\lambda/4$ stacks, respectively. The middle panel is the phononic dispersion of a $\lambda/8,3\lambda/8$ stack.

This parallel between the properties of light and sound can be evidenced through the photon and phonon dispersion of a periodic $\lambda/4,\lambda/4$ DBR, as shown in Fig. 2 (left and right panels). The wavelength of the two excitations is the same, but there is a contrasting energy scale due to the large difference between the speeds of sound and light. Nevertheless, the dispersion of one essentially mimics the other, characterized by zone folding with open gaps at the zone edge (indicated with arrows in the figure), and closed gaps at the zone center.

An ultrafast laser setup was used to study these cavity (confined) and slow (DBR) acoustic phonon modes in GaAs/AlAs microcavities. Time-resolved reflectivity experiments using degenerate ps-laser pump and probe [63] based on a delay line [see the scheme in Fig. 1(b)] were performed at room temperature. A single wavelength was used, exploiting the sample wedge to adjust it to either the optical cavity mode or the edge states. The laser wavelength was set so that the phonon generation and detection would be at resonance with the direct band gap of the GaAs making the cavity spacer ($E_{gap} \sim 1.425$ eV). Resonant coherent phonon generation experiments have been extensively used in the past for the study of layered semiconductor systems (see, for example, Refs. [64–67]) and for the selective excitation of confined acoustic vibrations in sound resonators [37,70]. Picosecond pulses (∼1 ps, ∼870.2 nm, ∼1.425 eV) from a mode-locked Ti:sapphire laser with a repetition rate 80 MHz were split into cross polarized pump (powers ranging from 10 to 20 mW) and probe (typically 1 mW) pulses. Photon pulses of 1 ps are chosen so that their spectral width matches approximately the finesse of the optical cavity ($\Delta\lambda \sim 1$ nm). Both pulses were focused onto superimposed ∼50-μm-diameter spots.

The coupling of light to the microcavity was done as described in Refs. [68,69]. The probe propagates close to the sample normal direction, while the pump incidence angle is set for double-resonant condition at the cavity mode [30,68]. With the pump and probe laser angles set in this way, the detuning between the laser and the cavity and edge modes was varied by displacing the laser spot on the sample surface.

III. TIME-RESOLVED REFLECTIVITY EXPERIMENTS

Typical spectra collected with the ps-laser setup and for different excitation conditions are shown in Fig. 3. These spectra are obtained from the Fourier transform of the time-resolved reflectivity traces, measured through the first 3 ns after the pump strikes the sample. The spectrum in the middle panel was obtained by resonantly exciting with the laser tuned to the cavity mode. Only three confined vibrational modes are observed, at ∼19, 58, and 96 GHz (highlighted with the red vertical bands). Almost identical spectra, albeit with varying intensity, are obtained when the laser detuning is varied around the optical cavity mode. The confined optical and phonon modes are localized in the same place of space, and it is this spatial confinement that explains the coupling of confined light to the confined acoustic modes. For the optical microcavity operating in the near infrared, the fundamental confined acoustic

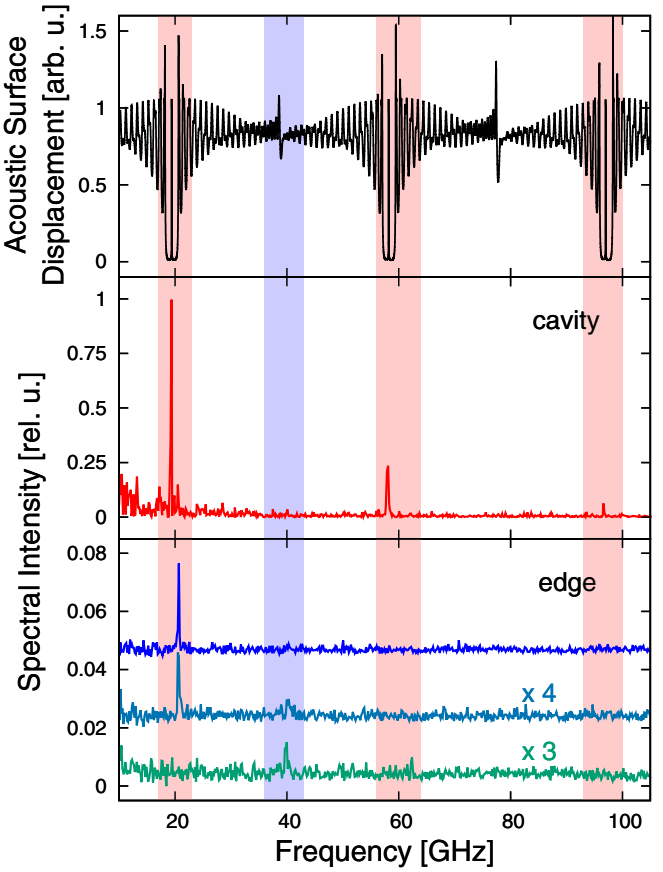

FIG. 3. Typical spectra obtained with ps-laser excitation tuned either with the cavity confined (center panel) or edge slow (bottom panel) optical modes. In the bottom panel three spectra obtained for different detunings within the edge optical band are displayed. Note that in the cavity case only acoustical cavity modes are observed (at ∼19, 58, and 96 GHz). When exciting through the edge optical modes, on the other hand, either pure confined, pure edge (∼40 GHz), or mixed phonon spectra are obtained depending on detuning. All amplitudes are given relative to that of the ∼20-GHz mode obtained with cavity mode laser excitation. The top panel displays the calculated surface displacement (related to the acoustic transmission), for acoustic phonons incident from the substrate side, to help identify the cavity (red bands) and edge (blue band) acoustic modes.

vibration falls in the $\Omega \approx 20$-GHz range, with higher-order modes being observable at frequencies given by $(2p+1)\Omega$ (p being an integer number). As shown in Figs. 2 and 3, even gaps are closed in $\lambda/4,\lambda/4$ mirrors, preventing the existence of the corresponding cavity modes. The observed modes correspond to z-polarized longitudinal acoustic phonons, more precisely the fundamental cavity breathing mode, and its third and fifth overtones, respectively [37]. Because these breathing modes correspond to the most efficient way of modulating the optical cavity mode, we also describe them as "nano-optomechanical modes." To help in the identification of these acoustic cavity modes the top panel of Fig. 3 shows the calculated surface displacement (related to the acoustic transmission) for phonons incident from the substrate. There are indeed well-developed stop bands with acoustic cavity modes close to 20, 60, and 100 GHz.

Contrastingly, the spectra are not only weaker when exciting through the edge optical states (bottom panel of Fig. 3) but also show qualitative variations depending on the precise laser detuning. This is illustrated for three characteristic cases in the figure, with spectra displaying either the acoustic cavity modes and particularly the more intense one at ∼21 GHz (top spectrum), a broader mode at ∼40 GHz (bottom spectrum), or both (middle spectrum). Note that the acoustic cavity modes for slow light excitation are blueshifted respect to the cavity resonant condition (top panel in Fig. 3). This shift results from the sample wedge that enables the optical state tuning but also modifies the confined acoustic vibration energies. The phonon mode at 40 GHz (highlighted with the blue band in Fig. 3) corresponds to a Brillouin-zone-center slow acoustic mode distributed throughout the DBR mirrors (we recall that the second minigap is closed, so that the second overtone of the fundamental cavity mode around 40 GHz is not expected) [71,72]. To understand the observation of this mode, we note that the microcavity can be viewed as two coupled finite-size periodic DBRs. According to coherent phonon selection rules for a periodic system, in the generation process light couples to $q_G = 0$ (zone-center) vibrations, while for the detection in back-scattering geometry light couples to $q_D = 2k$ modes (here q and k are the phonon and photon wave numbers, respectively) [30]. When exciting with a wavelength in resonance with the optical cavity mode, $k = \pi/d$, with d the DBR period. It follows that $q_D = 2\pi/d$, which has the same symmetry as a $q = 0$ mode. This implies that zone-center modes are generated and detected at the DBR. When exciting through the edge optical mode due to the thickness wedge this condition will be approximately met. Also because the DBR is finite, wave-vector conservation is expected to be partially relaxed (thus explaining also the observation of the confined mode at ∼21 GHz). But in any case, light will couple preferentially in the DBRs to modes close to Brillouin-zone center. We note, however, that due to the fact that for the studied $\lambda/4,\lambda/4$ mirrors the acoustic stop bands at the Brillouin-zone center are almost closed, the phonon slowing down for the observed 40-GHz mode is not optimized. We will address this point further below.

The color map in Fig. 4 presents the phonon spectral amplitude as a function of laser detuning around the optical cavity mode (the detuning here is defined as $\delta E = E_{\text{cav}} - E_{\text{laser}}$, with E the cavity or laser energy, respectively). The measured

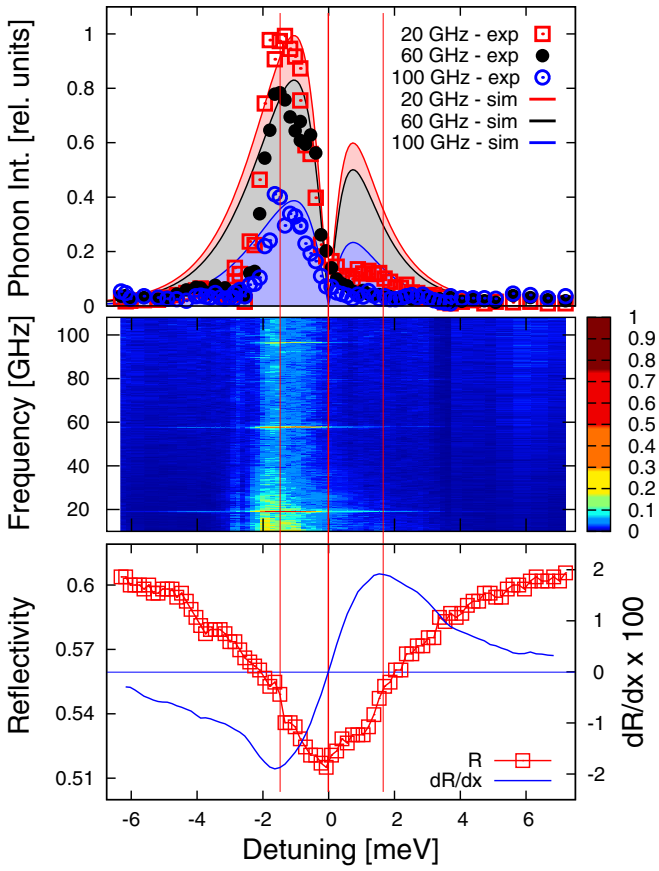

FIG. 4. Amplitude of the acoustic cavity modes obtained with the ps-laser wavelength tuned in the region around the optical cavity mode (confined light). The top and middle panels present the measured amplitude of the acoustic cavity modes as a function of detuning both as intensity curves (symbols) and color map, respectively. In the top panel the continuous lines are the calculated amplitudes (see text for details). All amplitudes are given with respect to the maximum obtained for the ∼20-GHz acoustic cavity mode. The bottom panel shows with symbols the optical reflectivity measured with the probe beam. The continuous curve is the numerical derivative of the measured reflectivity.

detuning dependence of the amplitude of the three observed acoustic phonon confined modes is shown with symbols in the top panel. All curves have been normalized to the maximum amplitude of the 20-GHz fundamental acoustic cavity mode. The bottom panel shows the measured probe optical reflectivity (symbols) and its smoothed numerical derivative (continuous curve). The absorption at the GaAs spacer layer, together with the broadening induced by the laser spectral width, explain the nonobservation of zero reflectivity at the cavity mode dip. The phonon amplitude maxima are observed at both optical cavity mode flanks where the reflectivity derivative is maximum, as described in Refs. [68,69]. At these positions the phonon detection sensitivity is maximum. The negative detuning flank is particularly enhanced because it is for this case that the double-resonant condition (pump tuned to the cavity mode) holds.

An experiment similar to that of Fig. 4 but with the laser tuned in the region of the optical DBR edge (slow) modes is

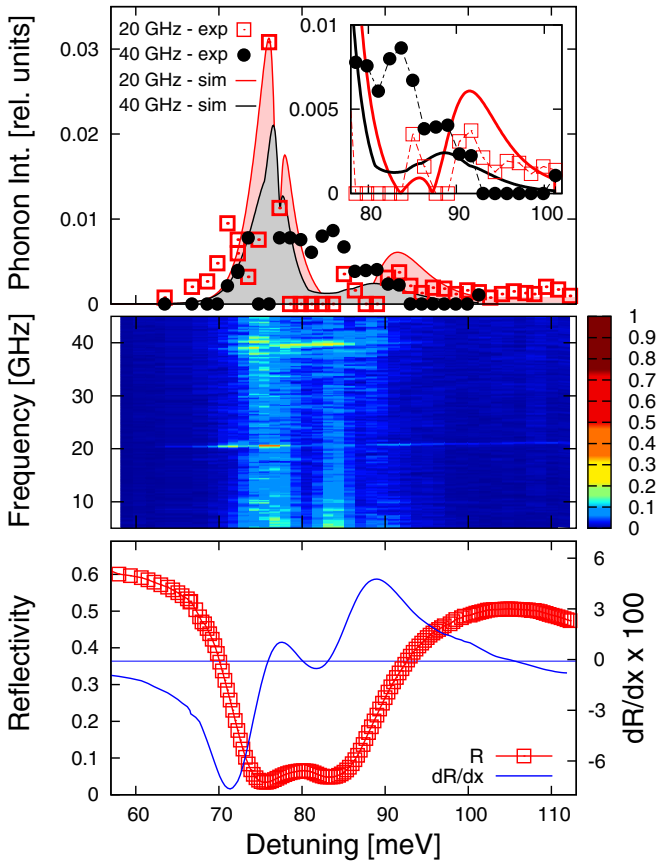

FIG. 5. Amplitude of the ∼20-GHz acoustic cavity mode and ∼40-GHz acoustic slow edge mode obtained with the ps-laser wavelength tuned in the region around the optical edge modes (slow light). We use exactly the same code as in Fig. 3. In the top panel the inset shows a detail of the high detuning region. All amplitudes are given with respect to the maximum obtained for the ∼20-GHz acoustic cavity mode with optical cavity mode excitation.

presented in Fig. 5. Again, the phonon intensity color map (center panel), the amplitude of two selected modes (top panel), and the measured probe optical reflectivity and its smoothed numerical derivative (bottom panel) are displayed. In this case there are two reflectivity minima in the region of the optical edge states, in agreement with the calculated curve in Fig. 1(a). These minima attain almost zero reflectivity. The edge bands are much broader than the cavity mode (nominal effective Q factor assuming no absorption ∼400 as compared to $Q \sim 4000$ for the cavity mode), and consequently the laser spectral width is not critical. The main observations here are the following: (i) the overall phonon amplitudes are around 1% of those obtained with cavity resonant excitation, and (ii) the intensity of the two observed modes follows a complex detuning dependence, with alternatively the confined, edge, or both acoustic modes being observed. All these observations, and the ones derived when describing Fig. 4, point to the importance of theoretically considering the consequences of the modified propagation of photons and phonons in these resonant optomechanic structures, something that we address next.

We proceed now to the analysis of the presented results with a model for pump-probe differential optical reflectivity that takes into account both the elastic and electromagnetic response of the layered structure (for a detailed description of the model see Refs. [67,72]). Standard transfer matrix formalisms were used to evaluate the electric-field distribution and the acoustic field distribution in the structure. Two terms are considered for the detection process, namely, one due purely to the photoelastic effect (i.e., a change in the index of refraction induced by strain), and another resulting from the displacement of the interfaces (i.e., an effective change in the thickness distribution of the structure) [37,73–75]. The interface displacement term is fully determined by a proper evaluation of the acoustic modes of the structure, and by physical constants (dielectric functions) that are readily available for most materials. The photoelastic constant p, on the other hand, has only been measured for a few materials, and even in those cases for a limited range of wavelengths [76]. Very recently its resonant dependence in GaAs multiple quantum wells has been described, evidencing huge (up to 10^5) polariton-mediated enhancement [77]. In the model it is assumed that the only perturbation to the structure reflectivity arises from the presence of the generated coherent phonons. The cavity mode is otherwise assumed to be fixed at its equilibrium position, determined by the materials' *equilibrium* index of refraction and layer thickness.

Published values were used for all required material parameters, complex dielectric functions, sound velocity, and mass density (see Table I). Nominal values were used for the layer thickness, uniformly augmented or decreased to account for the structure wedge, and chosen so that the calculated optical cavity mode energy would be consistent with the position dependent measured photoluminescence. A deformation potential (displacive) phonon generation mechanism was assumed, larger in the GaAs spacer (generation constant $K = 1$) as compared to the DBR $Al_{0.18}Ga_{0.82}As$ alloy ($K = 0.2$) because of the laser resonance with the GaAs gap (the gap of $Al_{0.18}Ga_{0.82}As$ at room temperatures is around ∼1.746 eV, well above the laser energy). The optoelectronic stress is assumed constant within the GaAs layer, not reflecting the oscillating half-wave spatial pattern of the pump field but only its average intensity. This reflects the assumption that the photoexcited carriers contributing to the deformation potential mechanism are very rapidly distributed within the full thickness of the GaAs layer after photoexcitation [78]. It turns out that this assumption is important to well describe the relative intensity of the observed acoustic cavity modes. Also because of the resonance with the GaAs gap, the photoelastic constants used were $p_{GaAs} = 6.0$ and $p_{AlGaAs} = 1.2$. The absolute magnitude of the generation constant K is not relevant: experimental and calculated curves are normalized to the maximum intensity

TABLE I. List of parameters used in the simulations.

Material	n	ρ (kg/m^3)	v_s (m/s)
GaAs	3.299	5.32	4730.0
$Al_{0.18}Ga_{0.82}As$	3.207	5.04	4860.2
AlAs	2.86	3.76	5650.0

of the 20-GHz mode measured with the laser tuned with the optical cavity mode. The absolute values of p (assumed as real) are more relevant, because of the interference between the photoelastic and geometrical (interface) terms in the detection process. Generation and photoelastic constants in AlAs were taken as zero, because of the large magnitude of the optical gap in this material ($\sim$3 eV).

The continuous curves in the top panels of Figs. 4 and 5 resume the main results of the model calculations, focusing on the detuning dependence of the amplitude of the different coherently generated acoustic phonons. We point first the attention to the laser excitation through the confined optical cavity mode (top panel in Fig. 4). Several features can be highlighted.

(i) A strong enhancement of the phonon signals is observed on excitation resonant with the cavity mode, and detection at the cavity mode flanks.

(ii) The shape of the detuning dependence for negative values, and relative magnitude of the confined modes, is well accounted for by the calculations. The spectra are essentially determined by the photoelastic term which is resonant at the spacer where the acoustic phonon modes are confined. The maximum intensity results from the optimization of the pump being tuned to the cavity mode, and the probe to its high derivative flank.

(iii) The relative magnitude of the acoustic confined modes is mainly determined by the detection sensitivity, which is proportional to the overlap between the phonon strain distribution, and the square of the cavity confined optical probe field. This overlap integral is similar for the 20- and 60-GHz vibrations, but rapidly decays for higher overtones because of the positive and negative lobes of the strain field within the spacer layer.

(iv) The agreement is not so good for positive detunings, where the predicted intensities are much larger than what is experimentally observed. This is mainly due to the limitations of the model, that does not account for the dynamics of the optical cavity mode after pump laser excitation. In fact, carrier absorption produces a large and rapid blueshift of the cavity mode after pump excitation, strongly modifying the detection sensitivity along the relaxation transients (see the detailed discussion in Ref. [38]). While the mode remains tuned at all times to the probe laser if it is at negative detunings before being perturbed, it is expelled out of the probe bandwidth for positive detunings. In this latter case the probe senses most of the time regions of the structure's reflectivity stop band that are essentially flat. This explains the observation of signals that are much smaller than predicted by the model for positive detunings.

The top panel in Fig. 5 presents the case of excitation through the edge (slow) optical modes. In this case it is observed that light couples both to confined ($\sim$20 GHz) and slow acoustic phonons ($\sim$40 GHz). As follows from this figure, a clear enhancement of the signals is observed on tuning the laser wavelength with the slow DBR optical modes. It is noteworthy the qualitative agreement between experiment and theory in the general trends of the detuning dependence of the coherent phonon intensity, including details of local peaks and dips as emphasized in the inset to the figure. The large variations of intensity result from a complex combination of effects, including the pump intensity within the structure, the position of the probe with respect to the regions of large reflectivity variations, and the relative phase between the electric-field distribution and the strain field of the specific mode under consideration. The relative intensity of the 20- and 40-GHz modes is well described by the model calculations, but not the relation between confined mode and slow light excitation. While the experimental ratio is 0.03, the theoretical model predicts a much contrasting relation of $\sim 8 \times 10^{-4}$ between the intensity using slow light as compared to confined light. In fact, the absolute values of the calculated curves in this figure have been scaled to fit the maximum intensity of the 20-GHz mode. We believe that the origin of this discrepancy (experimental 0.03 versus calculated $\sim 8 \times 10^{-4}$) is again related to point (iv) discussed above, and the different effective Q factors of optical cavity and edge modes. In fact, carrier induced transient shifts of the cavity mode amounting to a couple of meV are critical when sensing with a probe laser of $\sim 1-2$-meV spectral width and with a cavity mode with spectral width also of the order of a meV. In contrast, the edge modes have widths on the order of 10 meV. Consequently, for laser excitation through the edge optical modes the "frozen" model used is much better justified, providing a good description of the processes involved.

The resonant behavior presented in Fig. 5 demonstrates the effect of slowing light on the coupling between photons and slow acoustic phonons in a photonic one-dimensional crystal. What is not obvious from these results is the role played by the slowing down of the phonons in the optophononic process. In fact, as already discussed above when describing the top panel in Fig. 2, for the studied structure which was optimized to perform as an optical microcavity, with $(\lambda/4,\lambda/4)$ optical DBRs, the acoustic gap around 40 GHz (zone center) is almost closed. Consequently, one does not expect in this case a significant acoustic phonon slowing down. The question then arises: is it possible to optimize the structure design so that optical excitation through a slow optical mode is compatible with a substantial slowing down of the acoustic phonon mode to which such optical modes couple?

As discussed in Ref. [39], and is illustrated for the acoustic case in Fig. 2 (center), the first Brillouin-zone-center gaps are optimized for $(3\lambda/8,\lambda/8)$ structures. This applies equivalently to sound or optical waves. The top panel in Fig. 6 shows the continuous variation of the first Brillouin-zone-center acoustic minigap when the thicknesses of the layers of a DBR are varied away from $(3\lambda/8,\lambda/8)$, and up to the previously studied symmetric case $(\lambda/4,\lambda/4)$, keeping the total thickness of the period constant. These calculations were performed for an infinite $Al_{0.18}Ga_{0.82}As$ /AlAs DBR, with layer thickness set so that the laser tuned at 870-nm wavelength is resonant with the higher-energy first zone-center optical edge mode. The layer thicknesses vary from (134/144) to (201/72) nm (the used indices of refraction are given in Table I). The violet thicker curve corresponds to the previously discussed symmetric case; the red curve corresponds to the $(3\lambda/8,\lambda/8)$ situation. The progressive opening of the acoustic minigap, and flattening of the acoustic dispersion at the zone center (implying sound speed reduction) is evident. The middle panel in Fig. 6 displays the calculated wavelength dependence of the surface displacement for a phonon incident from the substrate

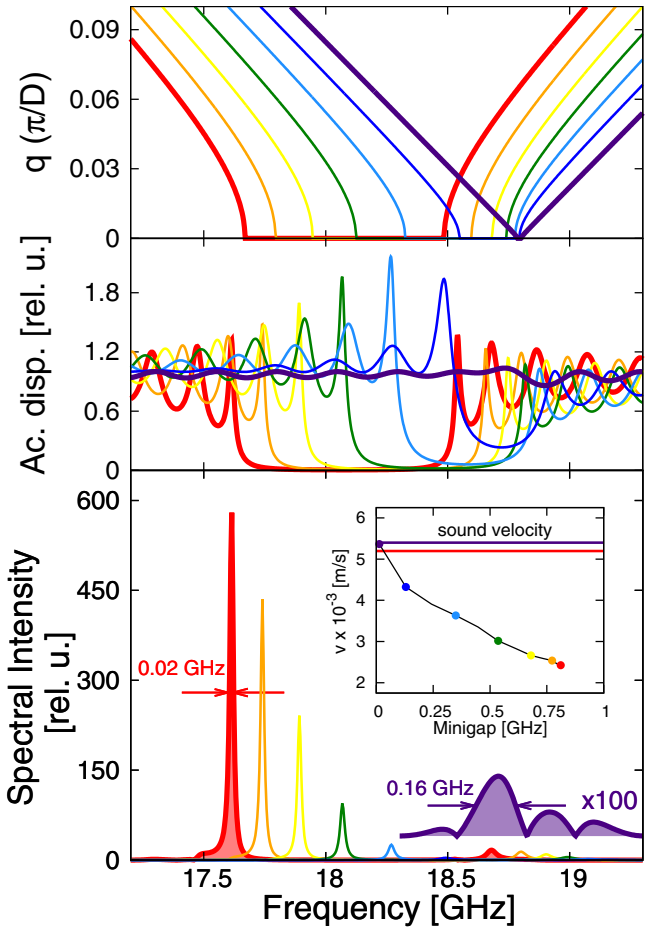

FIG. 6. Model calculation for the optimized coupling between slow light and slow acoustic phonons in a DBR. The top panel shows the acoustic dispersion close to the first zone center gap for infinite periodic $Al_{0.18}Ga_{0.82}As$ /AlAs DBRs of varying structure. The thickness of the DBR layers varies for the different curves away from the optical $(\lambda/4,\lambda/4)$ condition and up to $(3\lambda/8,\lambda/8)$, but keeping the lattice period unchanged [the black curves in the three panels correspond to the $(\lambda/4,\lambda/4)$ case; the red ones correspond to $(3\lambda/8,\lambda/8)$]. The middle panel is the surface displacement for acoustic phonons incident from the substrate side for DBRs of the same structure as in the top panel, but limited to 38 periods. The bottom panel shows the calculated coherent phonon spectral intensity corresponding to differential reflectivity experiments with edge mode optical excitation in these same structures. The inset in this panel is the sound velocity evaluated at the maxima of the slow phonon peaks (see text for details).

(equivalent to the phonon transmission) for a 38 period finite DBR, with the same structure as the curves in the top panel, and grown on a GaAs substrate. The opening of the acoustic minigap (tranmission stop band) is again evidenced, with a slight progressive blueshift of the minigap center due to the change in the structure's sound velocity. Note that the edge modes do not fall exactly at the position of the phonon dispersion minigaps of the infinite structure (top panel) due to finite-size effects [79].

The bottom panel in Fig. 6 displays the calculated coherent phonon spectra for a reflectance difference experiment as discussed above. The spectra were calculated for optical excitation at the high-energy edge state of the first zone-center optical gap where the intensity is maximum. These slow optical edge modes are localized (standing) waves with effective wave vector $k = 0$. Thus, the selection rules for coupling to the DBR vibrations discussed above imply that these optical slow modes couple very efficiently to the zone-center $q = 0$ slow phonons. The main peak corresponds to the $q_D \sim 0$ (zone center, slow mode) contribution. It is quite notable the simultaneous strong enhancement and narrowing of the peak associated to the slow phonon state. The magnitudes are given with respect to the intensity of the slow phonon mode for the symmetric $(\lambda/4,\lambda/4)$ structure. The latter (shown with a violet thicker curve) has been multiplied by 100 in the figure to make it visible with respect to the strongly amplified $(3\lambda/8,\lambda/8)$ case (red curve). The observed narrowing of the $q_D \sim 0$ phonon peak reflects the flattening of the band dispersion, the related reduction of sound speed, and concomitantly the increased lifetime of the vibrations within the DBR. The change of sound speed, derived from the phonon dispersion shown in the top panel of Fig. 6, and evaluated at the spectral position of the phonon peaks shown in the bottom panel of the same figure, are shown as an inset to the latter. The horizontal violet and red lines correspond to the sound speed away from the Bragg gaps (i.e., in the linear regions) of the symmetric $(\lambda/4,\lambda/4)$ and $(\lambda/8,3\lambda/8)$ structure, respectively.

The signal enhancement observed in Fig. 6 (almost a factor $\times 600$) is mainly due to the combined effects associated to the strong localization of both the strain and the electric field within the DBRs. In fact the evolution from a $(\lambda/4,\lambda/4)$ to a $(3\lambda/8,\lambda/8)$ structure derives in the simultaneous opening of *both* phononic and photonics first zone-center gaps. The calculations show that, concomitant with this gap opening, both the strain fields and electric-field intensity increase by a factor of 4 approximately. The generation and the detection terms in a reflectance difference experiment are the two proportional to the strain field and electric-field square [67]. Consequently it is these contributions of magnitude $\sim 4^4$ that explain most of the factor $\times 600$ increase of the signal induced by the slowing down of light and sound. The difference is presumably due to a better phase matching in the $(3\lambda/8,\lambda/8)$ case between the two fields, and the regions with larger GaAs content (and consequently larger generation and photoelastic constants).

We conclude from the previous discussion that the combined enhancement of the phonon-photon coupling due to spatial localization contributes synergically to a strong enhancement of the optomechanical processes in these optimized one-dimensional photonic crystals. What remains to be discussed is the comparison of such a slow light-sound structure with a resonant microcavity with similar number of layers. To do this we evaluate the optomechanical response of the $(3\lambda/8,\lambda/8)$ DBR structure described above, with a microcavity made by opening a $\lambda/2$ GaAs spacer so that 20 DBR periods remain as bottom mirror (next to the GaAs substrate) and 18 periods are left on top. The resulting squared electric and strain fields are shown in the top and middle panels of Fig. 7, respectively. For the microcavity the optical excitation is evaluated in double resonance with the cavity mode, as discussed for the experiments above.

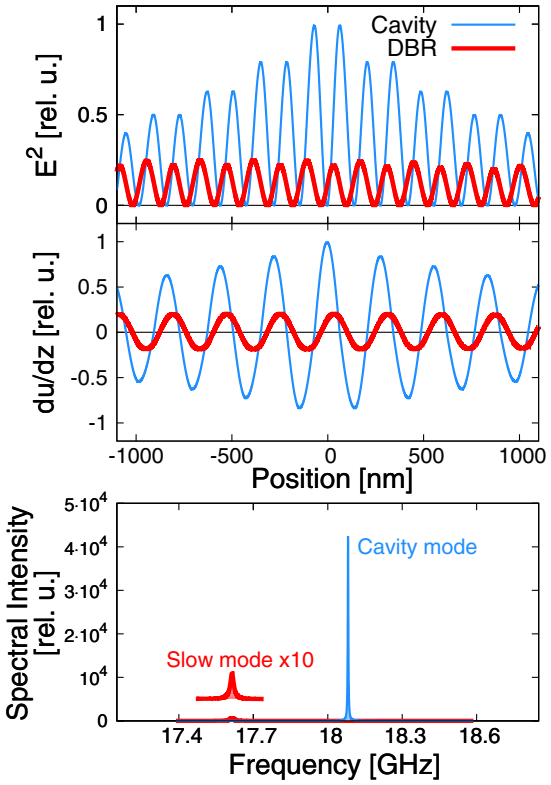

FIG. 7. Comparison between the reflectance difference signal of a 38 period ($3\lambda/8,\lambda/8$) DBR structure (as presented in Fig. 6), and a microcavity made by opening a $\lambda/2$ GaAs spacer in the latter. The top and middle panels display the calculated squared electric and strain fields, respectively. The magnitudes are given relative to the maximum of the microcavity case. The bottom panel shows the corresponding calculated reflectance difference signal, with the same scale as the bottom panel in Fig. 6 (see text for details).

Quite notably, the resonant confinement induced by simply introducing a cavity mode in the gap leads to a factor of 4 further enhancement both in the strain and squared electric fields, when compared to the DBR structure. The resulting coherent phonon signal is amplified by $\times 70$ in the cavity with respect to the bare DBR, somewhat smaller than the factor $E^4(du/dz)^2 \approx 4^4$ because of the larger spatial extension of the slow optical and vibrational modes, with respect to the confined ones.

IV. CONCLUSIONS

In conclusion, we introduced the idea of using slow light modes to sense slow acoustic phonon modes that are otherwise not accessible in semiconductor one-dimensional photonic crystals and cavities. Up to now, mostly confined modes have been used in optomechanics. We have shown that semiconductor DBR-based microcavities display both confined and slow light and confined and slow acoustic phonons as a rich playground for such optomechanical coupling, with the added interest of accessing relatively high-frequency vibrations (20–100 GHz). This work is a fundamental step towards the exploration of such novel measuring schemes and applications. We have studied the coupling between such confined and slow light with confined and slow phonons using time-resolved reflectance difference spectroscopies in one-dimensional optical microcavities. The experiments were compared with calculations using a model that takes into account the precise distribution of light and acoustic fields in the resonant device.

The experiments demonstrate that both confinement and slowing down of light and acoustic phonons contribute to strongly enhancing the interaction of photons with phonons. It is shown that confined light couples only to confined sound in these devices, while slow light couples both to confined and slow vibrational modes. The optomechanical coupling efficiency in the experimentally studied device with ($\lambda/4,\lambda/4$) DBRs and cavity mode Q factors in the range of 1000 is orders of magnitude larger exploiting light and sound confinement than through the slowing down at the stop-band edges. It is predicted, however, that better optomechanical cooperativity could be attained if the structures are optimized for the simultaneous slowing down of light and acoustic phonons in the same place of space.

It has been recently shown [58] that by introducing a slow light medium into an optical microresonator, the lifetime of a photon circulating in the device can be extended by several orders of magnitude and up to the millisecond range, a range that is characteristic of or even larger than the lifetime of phonons. Our results indicate that such synergic combination of speed reduction and confinement could open the path to improved optomechanical devices.

ACKNOWLEDGMENT

This work was partially supported by the ANPCyT Grants PICT 2012-1661 and 2013-2047, the French RENATECH network, the international franco-argentinean laboratory LIFAN (CNRS-CONICET), a public grant overseen by the French National Research Agency (ANR) as part of the "Investissements d'Avenir" program (Labex NanoSaclay, reference: ANR-10-LABX-0035), and the grant ANR QDOM. N.D.L.K. was supported by the FP7 Marie Curie Fellowship OMSiQuD.

[1] O. Arcizet, P.-F. Cohadon, T. Briant, M. Pinard, and A. Heidmann, Nature (London) **444**, 71 (2006).
[2] T. J. Kippenberg and K. J. Vahala, Science **321**, 1172 (2008).
[3] J. D. Thompson, B. M. Zwickl, A. M. Jayich, F. Marquardt, S. M. Girvin, and J. G. E. Harris, Nature (London) **452**, 72 (2008).
[4] M. Eichenfield, J. Chan, R. M. Camacho, K. J. Vahala, and O. Painter, Nature (London) **462**, 78 (2009).
[5] M. S. Kang, A. Nazarkin, A. Brenn, and P. St. J. Russell, Nat. Phys. **5**, 276 (2009).
[6] I. Favero and K. Karrai, Nat. Photonics **3**, 201 (2009).
[7] F. Marquardt and S. M. Girvin, Physics **2**, 40 (2009).

[8] S. Groeblacher, K. Hammerer, M. R. Vanner, and M. Aspelmeyer, Nature (London) **460**, 724 (2009).

[9] A. Schliesser, O. Arcizet, R. Riviere, and T. J. Kippenberg, Nat. Phys. **5**, 509 (2009).

[10] S. Weis, R. Riviere, S. Deleglise, O. Arcizet, E. Gavartin, A. Schliesser, and T. J. Kippenberg, Science **330**, 1520 (2010).

[11] Q. Lin, J. Rosenberg, D. Chang, R. Camacho, M. Eichenfield, K. J. Vahala, and O. Painter, Nat. Photon. **4**, 236 (2010).

[12] A. D. O'Connell, M. Hofheinz, M. Ansmann, Radoslaw C. Bialczak, M. Lenander, Erik Lucero, M. Neeley, D. Sank, H. Wang, M. Weides, J. Wenner, John M. Martinis, and A. N. Cleland, Nature (London) **464**, 697 (2010).

[13] J. D. Teufel, T. Donner, Dale Li, J. H. Harlow, M. S. Allman, K. Cicak, A. J. Sirois, J. D. Whittaker, K. W. Lehnert, and R. W. Simmonds, Nature (London) **475**, 359 (2011).

[14] J. Chan, T. P. Mayer Alegre, Amir H. Safavi-Naeini, Jeff T. Hill, Alex Krause, Simon Groeblacher, Markus Aspelmeyer, and Oskar Painter, Nature (London) **478**, 89 (2011).

[15] E. Verhagen, S. Deleglise, S. Weis, A. Schliesser, and T. J. Kippenberg, Nature (London) **482**, 63 (2012).

[16] J. D. Teufel, T. Donner, M. A. Castellanos-Beltran, J. W. Harlow, and K. W. Lehnert, Nature Nanotechnology **4**, 820 (2009).

[17] B. P. Abbott *et al.* (LIGO Scientific Collaboration and Virgo Collaboration), Phys. Rev. Lett. **116**, 131103 (2016) and references therein.

[18] C. Zhao, L. Ju, H. Miao, S. Gras, Y. Fan, and D. G. Blair, Phys. Rev. Lett. **102**, 243902 (2009).

[19] I. S. Grudinin, H. Lee, O. Painter, and K. J. Vahala, Phys. Rev. Lett. **104**, 083901 (2010).

[20] A. Kavokin and G. Malpuech, *Cavity Polaritons* (Elsevier, Amsterdam, 2003).

[21] Semicond. Sci. Technol. **18**, S279 (2003), special issue on microcavities, edited by J. J. Baumberg and L. Viña.

[22] See, for example, E. Wertz, L. Ferrier, D. D. Solnyshkov, R. Johne, D. Sanvitto, A. Lemaitre, I. Sagnes, R. Grousson, A. V. Kavokin, P. Senellart, G. Malpuech, and J. Bloch, Nat. Phys. **6**, 860 (2010).

[23] A. Dousse, J. Suffczynski, A. Beveratos, O. Krebs, A. Lemaitre, I. Sagnes, J. Bloch, P. Voisin, and P. Senellart, Nature (London) **466**, 217 (2010).

[24] N. Somaschi, V. Giesz, L. De Santis, J. C. Loredo, M. P. Almeida, G. Hornecker, S. L. Portalupi, T. Grange, C. Antn, J. Demory, C. Gómez, I. Sagnes, N. D. Lanzillotti-Kimura, A. Lemaître, A. Auffeves, A. G. White, L. Lanco, and P. Senellart, Nature Photonics **10**, 340 (2016).

[25] T. Someya, R. Werner, A. Forchel, M. Catalano, R. Cingolani, and Y. Arakawa, Science **285**, 1905 (1999).

[26] A. Fainstein, B. Jusserand, and V. Thierry-Mieg, Phys. Rev. Lett. **75**, 3764 (1995).

[27] A. Fainstein, B. Jusserand, and V. Thierry-Mieg, Phys. Rev. Lett. **78**, 1576 (1997).

[28] A. Fainstein, B. Jusserand, and V. Thierry-Mieg, Phys. Rev. B **53**, R13287 (1996).

[29] A. Fainstein and B. Jusserand, Phys. Rev. B **57**, 2402 (1998).

[30] N. D. Lanzillotti-Kimura, A. Fainstein, A. Huynh, B. Perrin, B. Jusserand, A. Miard, and A. Lemaitre, Phys. Rev. Lett. **99**, 217405 (2007).

[31] Y. Li, Q. Miao, A. V. Nurmikko, and H. J. Maris, J. Appl. Phys. **105**, 083516 (2009).

[32] M. M. de Lima, Jr., R. Hey, P. V. Santos, and A. Cantarero, Phys. Rev. Lett. **94**, 126805 (2005).

[33] M. M. de Lima, Jr., M. van der Poel, P. V. Santos, and J. M. Hvam, Phys. Rev. Lett. **97**, 045501 (2006); E. A. Cerda-Mendez, D. N. Krizhanovskii, M. Wouters, R. Bradley, K. Biermann, K. Guda, R. Hey, P. V. Santos, D. Sarkar, and M. S. Skolnick, *ibid.* **105**, 116402 (2010).

[34] A. V. Scherbakov, T. Berstermann, A. V. Akimov, D. R. Yakovlev, G. Beaudoin, D. Bajoni, I. Sagnes, J. Bloch, and M. Bayer, Phys. Rev. B **78**, 241302(R) (2008).

[35] T. Czerniuk, C. Brugemann, J. Tepper, S. Brodbeck, C. Schneider, M. Kamp, S. Holing, B. A. Glavin, D. R. Yakovlev, A. V. Akimov, and M. Bayer, Nat. Commun. **5**, 4038 (2014).

[36] T. Czerniuk, J. Tepper, A. V. Akimov, S. Unsleber, C. Schneider, M. Kamp, S. Hoefling, D. R. Yakovlev, and M. Bayer, Appl. Phys. Lett. **106**, 041103 (2015).

[37] A. Fainstein, N. D. Lanzillotti-Kimura, B. Jusserand, and B. Perrin, Phys. Rev. Lett. **110**, 037403 (2013).

[38] P. Sesin, P. Soubelet, V. Villafañe, A. E. Bruchhausen, B. Jusserand, A. Lemaítre, N. D. Lanzillotti-Kimura, and A. Fainstein, Phys. Rev. B **92**, 075307 (2015).

[39] M. Trigo, A. Bruchhausen, A. Fainstein, B. Jusserand, and V. Thierry-Mieg, Phys. Rev. Lett. **89**, 227402 (2002).

[40] S. Anguiano, G. Rozas, A. E. Bruchhausen, A. Fainstein, B. Jusserand, P. Senellart, and A. Lemaître, Phys. Rev. B **90**, 045314 (2014).

[41] M. Notomi, K. Yamada, A. Shinya, J. Takahashi, C. Takahashi, and I. Yokohama, Phys. Rev. Lett. **87**, 253902 (2001).

[42] A. Figotin and I. Vitebskiy, Phys. Rev. E **74**, 066613 (2006).

[43] Y. Chen, J. Rosenkrantz de Lasson, N. Gregersen, and Jesper Mrk, Phys. Rev. A **92**, 053839 (2015)

[44] O. Deparis, S. R. Moucheta, and B.-L. Su, Phys. Chem. Chem. Phys. **17**, 30525 (2015).

[45] P. Lodahl, A. Floris van Driel, I. S. Nikolaev, A. Irman, K. Overgaag, D. Vanmaekelbergh, and W. L. Vos, Nature (London) **430**, 654 (2004).

[46] A. V. Balakin, V. A. Bushuev, B. I. Mantsyzov, I. A. Ozheredov, E. V. Petrov, A. P. Shkurinov, P. Masselin, and G. Mouret, Phys. Rev. E **63**, 046609 (2001).

[47] Y. Dumeige, I. Sagnes, P. Monnier, P. Vidakovic, I. Abram, C. Mériadec, and A. Levenson, Phys. Rev. Lett. **89**, 043901 (2002).

[48] M. Soljacic, S. G. Johnson, S. Fan, M. Ibanescu, E. Ippen, and J. D. Joannopoulos, J. Opt. Soc. Am. B **19**, 2052 (2002).

[49] Mohamed A. K. Othman, Farshad Yazdi, Alex Figotin, and Filippo Capolino, Phys. Rev. B **93**, 024301 (2016).

[50] Saikat Ghosh, Jay E. Sharping, Dimitre G. Ouzounov, and Alexander L. Gaeta, Phys. Rev. Lett. **94**, 093902 (2005).

[51] G. Vecchi, F. Raineri, I. Sagnes, A. Yacomotti, P. Monnier, T. J. Karle, K.-H. Lee, R. Braive, L. Le Gratiet, S. Guilet, G. Beaudoin, A. Talneau, S. Bouchoule, A. Levenson, and R. Raj, Opt. Express **15**, 7551 (2007).

[52] Weiqi Xue, Yi Yu, Luisa Ottaviano, Yaohui Chen, Elizaveta Semenova, Kresten Yvind, and Jesper Mork, Phys. Rev. Lett. **116**, 063901 (2016).

[53] James F. McMillan, Xiaodong Yang, Nicolae C. Panoiu, Richard M. Osgood, and Chee Wei Wong, Opt. Lett. **31**, 1235 (2006).

[54] K. Inoue, H. Oda, A. Yamanaka, N. Ikeda, H. Kawashima, Y. Sugimoto, and K. Asakawa, Phys. Rev. A **78**, 011805(R) (2008).

[55] K. Kondo and T. Baba, Phys. Rev. A **93**, 011802(R) (2016).

[56] C. Mechri, P. Ruello, and V. Gusev, New J. Phys. **14**, 023048 (2012).
[57] Tian-Xue Ma, Yue-Sheng Wang, Chuanzeng Zhang, and Xiao-Xing Su, J. Opt. **16**, 085002 (2014).
[58] V. Huet, A. Rasoloniaina, P. Guillemé, P. Rochard, P. Féron, M. Mortier, A. Levenson, K. Bencheikh, A. Yacomotti, and Y. Dumeige, Phys. Rev. Lett. **116**, 133902 (2016).
[59] A. Tredicucci, Y. Chen, V. Pellegrini, M Börger, L. Sorba, F. Beltram, and F. Bassani, Phys. Rev. Lett. **75**, 3906 (1995).
[60] A. Fainstein, B. Jusserand, P. Senellart, J. Bloch, V. Thierry-Mieg, and R. Planel, Phys. Rev. B **62**, 8199 (2000).
[61] A. Huynh, N. D. Lanzillotti-Kimura, B. Jusserand, B. Perrin, A. Fainstein, M. F. Pascual-Winter, E. Peronne, and A. Lemaître, Phys. Rev. Lett. **97**, 115502 (2006).
[62] M. Trigo, T. A. Eckhause, M. Reason, and R. S. Goldman, and R. Merlin, Phys. Rev. Lett. **97**, 124301 (2006).
[63] C. Thomsen, H. T. Grahn, H. J. Maris, and J. Tauc, Phys. Rev. B **34**, 4129 (1986).
[64] A. Bartels, T. Dekorsy, H. Kurz, and K. Kohler, Phys. Rev. Lett. **82**, 1044 (1999).
[65] K. Mizoguchi, M. Hase, S. Nakashima, and M. Nakayama, Phys. Rev. B **60**, 8262 (1999).
[66] O. Matsuda and O. B. Wright, J. Opt. Soc. Am. B **19**, 3028 (2002).
[67] M. F. Pascual-Winter, A. Fainstein, B. Jusserand, and B. Perrin, and A. Lemaître, Phys. Rev. B **85**, 235443 (2012)
[68] N. D. Lanzillotti-Kimura, A. Fainstein, B. Perrin, and B. Jusserand, Phys. Rev. B **84**, 064307 (2011).
[69] N. D. Lanzillotti-Kimura, A. Fainstein, B. Perrin, B. Jusserand, L. Largeau, O. Mauguin, and A. Lemaître, Phys. Rev. B **83**, 201103(R) (2011).
[70] M. F. Pascual Winter, G. Rozas, A. Fainstein, B. Jusserand, B. Perrin, A. Huynh, P. O. Vaccaro, and S. Saravanan, Phys. Rev. Lett. **98**, 265501 (2007).
[71] N. D. Lanzillotti-Kimura, A. Fainstein, B. Jusserand, and A. Lemaître, Phys. Rev. B **79**, 035404 (2009).
[72] V. Villafañe, A. E. Bruchhausen, B. Jusserand, P. Senellart, A. Lemaître, and A. Fainstein, Phys. Rev. B **92**, 165308 (2015).
[73] C. Baker, W. Hease, Dac-Trung Nguyen, A. Andronico, S. Ducci, G. Leo, and I. Favero, Opt. Express **22**, 14072 (2014).
[74] P. T. Rakich, P. Davids, and Z. Wang, Opt. Express **18**, 14439 (2010).
[75] P. T. Rakich, C. Reinke, R. Camacho, P. Davids, and Z. Wang, Phys. Rev. X **2**, 011008 (2012).
[76] N. Lanzillotti-Kimura, A. Fainstein, and B. Jusserand, Ultrasonics **56**, 80 (2015).
[77] B. Jusserand, A. N. Poddubny, A. V. Poshakinskiy, and A. Fainstein, and A. Lemaître, Phys. Rev. Lett. **115**, 267402 (2015).
[78] P. Ruello and V. E. Gusev, Ultrasonics **56**, 21 (2015).
[79] M. Trigo, A. Fainstein, B. Jusserand, and V. Thierry-Mieg, Phys. Rev. B **66**, 125311 (2002).